

# Fermi surface of ferromagnetic $\text{EuB}_6$

R. G. Goodrich

*Department of Physics and Astronomy, Louisiana State University, Baton Rouge, Louisiana 70803-4001*

N. Harrison

*National High Magnetic Field Laboratory, Los Alamos National Laboratory, Los Alamos, New Mexico 87545*

J. J. Vuillemin

*Department of Physics, University of Arizona, Tucson, Arizona 85721*

A. Teklu

*Department of Physics and Astronomy, Louisiana State University, Baton Rouge, Louisiana 70803-4001*

D. W. Hall, Z. Fisk, and D. Young

*National High Magnetic Field Laboratory, Florida State University, Tallahassee, Florida 32310*

J. Sarrao

*Los Alamos National Laboratory, Los Alamos, New Mexico 87545*

(Received 29 June 1998)

We have determined the Fermi surface and effective masses of electronic carriers in ferromagnetic  $\text{EuB}_6$  from pulsed field magnetization and steady field torque Landau quantum oscillatory measurements. To aid in the interpretation of the measurements, superconducting quantum interference device magnetometer measurements of the overall magnetization were made on the same samples. The results are consistent with recent electronic structure calculations and show both an electron and a hole pocket located at the  $X$  point in the Brillouin zone. [S0163-1829(98)03945-9]

## I. INTRODUCTION

Over the past two decades the rare-earth hexaborides have been under increasingly detailed scrutiny, both experimentally and theoretically.<sup>1-6</sup> The reason for this interest is that this system of materials, all of which have cubic crystal structures similar to  $\text{CsCl}$ , exhibit varying electron correlation properties ranging from a heavy Fermion metal ( $\text{CeB}_6$ ) to a normal metal ( $\text{LaB}_6$ ), semiconductors ( $\text{SrB}_6$ ) to Kondo insulators ( $\text{SmB}_6$ ), and materials that show large variations in their electrical, magnetic, and thermal properties as a function of temperature and applied magnetic fields.

The magnetic, electrical, and thermal properties of  $\text{EuB}_6$  have been studied by several groups for a number of years. Near 15 K  $\text{EuB}_6$  undergoes a (high temperature) semiconductor to a (low temperature) semimetal transition; the same temperature  $\Theta_c$  at which it becomes ferromagnetic.<sup>2</sup> This transition is accompanied by a large blueshift in the plasma frequency.<sup>7</sup> The nature of the ferromagnetic state in this material has been a subject of controversy, having first been thought to be a simple collinear ferromagnet from neutron diffraction measurements.<sup>5</sup> The type of coupling mechanism between Eu spins has been variously suggested to be superexchange,<sup>4</sup> the Bloembergen-Rowland interaction,<sup>8-10</sup> and the Ruderman-Kittel-Kasuya-Yosida (RKKY) interaction.<sup>6</sup> Recently it was suggested that magnetic polarons are formed, and a signature of this state was found in Raman scattering studies.<sup>11</sup> In Ref. 11 it also is suggested that  $\text{EuB}_6$  should fall within the category of colossal magnetoresistance

materials. An extensive study of the magnetic and structural properties of the ferromagnetic transition in  $\text{EuB}_6$  reveals two transitions occurring within 3 K at zero applied field.<sup>12</sup> Finally, recent band structure calculations<sup>13</sup> show that, in the ferromagnetic state,  $\text{EuB}_6$  should be a compensated metal with both the electron and the hole Fermi surface (FS) sheets centered at the  $X$  point of the Brillouin zone (BZ).

In this paper we present the results of de Haas-van Alphen (dHvA) measurements on  $\text{EuB}_6$  in the ferromagnetic state. Other investigators have reported observation of field-dependent oscillatory behavior of the electrical resistance<sup>6</sup> [Shubnikov-de Haas (SdH) effect] but no complete picture of the FS previously has been given.

## II. EXPERIMENT

The measurements reported here were made on small single crystals in the shape of square rods having approximate dimensions of  $0.25 \text{ mm} \times 0.25 \text{ mm} \times 1 \text{ mm}$  long. Each of these dimensions was along a  $\langle 100 \rangle$ , or equivalent, axis of the cubic structure, and the magnetic field was applied along the cylinder axis for the magnetization measurements and perpendicular to the long axis for the torque measurements. The crystals were grown by the aluminum flux technique, and no visible signs of Al inclusion were evident upon magnification.

The dHvA magnetization measurements were made at the pulsed field facility of the National High Magnetic Field Laboratory (NHMFL) located at the Los Alamos National

Laboratory. The magnet used had a rise time from zero to 50 T of approximately 8 ms and the field decreased to zero in 25–30 ms. Field measurements were made by integrating the pickup voltage from a coil separate from the sample coil  $V_p$  over the time interval of the pulse. This voltage is proportional to  $dB/dt$ , thus,  $B(t) = C \int (dB/dt) dt$ , where  $C = NA$ , and  $N$  is the number of turns and  $A$  is the area exposed to the field during the measurement. Since  $NA$  is only approximately known because all exposed areas between leads going to the coil contribute to the voltage, the field conversion factor  $C$  was calibrated by measuring the dHvA frequencies of the well known orbits observed in Au.<sup>14</sup> From the Au data, the value of  $C$  was adjusted until these known frequencies were reproduced to within 0.1%.

The sample pickup coil was a small solenoid made from 640 turns of number 52 copper wire (diameter=0.016 mm) wound with an inner diameter of the solenoid equal to 1 mm. A counter wound cancellation coil was wound co-axially on the outer diameter of the central pickup coil to form an astatic pair. The number of turns on the cancellation coil was adjusted to give better than one turn empty coil cancellation for the pair. The two coils were connected to an external, low input impedance, voltage balancing and amplification circuit with a total gain in the net pickup voltage of 2500. When the sample was inserted into the coil, its overall magnetic moment in fields greater than 1 T caused a large imbalance in the pickup coil pair. With the external balancing circuitry we were able to reduce this imbalance at fields  $>1$  T to  $<1$   $\mu\text{V}$  before amplification.

The output of the amplifier was digitized with 12 bit resolution at a rate of 500 kHz, or 500 data points per mS, over the duration of the pulse. This rate gives 4000 data points on the up sweep and 12 500 on the down sweep. If one assumes, as an approximation, the field is linear in time for both the rising and falling parts of the pulse, the field resolution on the up-sweep is roughly 15 mT and on the down sweep 3 mT. In order to avoid any heating of the sample due to induced currents on the high sweep rate up-sweep, and to take advantage of the higher field resolution on the slower down sweeps, only the down sweep data were used for frequency and mass determinations.

Measurements were made between 0.4 and 4 K with the sample immersed in either a pumped  $^3\text{He}$  or  $^4\text{He}$  bath. The temperature of the sample was recorded at the beginning of the field pulse by measuring the resistance of a calibrated Cernox thermometer, as well as the vapor pressure of the bath. The amplitude of the dHvA signals was always larger on the increasing field side of the pulse, where  $dB/dt$  is the largest but eddy current heating would also be the largest, than on the smaller  $dB/dt$  falling side of the pulse. This fact indicates that very little heating of the sample due to induced currents was occurring, and that the mass measurements that depend on knowing the temperature of the sample during the pulse were accurate.

Angular-dependent torque measurements were made using a cantilever magnetometer between 12 and 24 T at the NHMFL, Tallahassee, FL. A five micron thick silicon cantilever was used<sup>15,16</sup> and was situated inside a brass can. The cantilever probe allowed for *in situ* rotation of the sample. The deflection of the cantilever was measured capacitively using a General Radio 1616 capacitance bridge and an

EG&G 124 lock-in-amplifier. Measurements were made in pumped  $^4\text{He}$  with the magnet sweeping at a rate of 0.5 T/min. The sensitivity of the cantilever increases linearly with applied field, and the amplitude of the torque term in the oscillatory part of the magnetization is proportional to  $dF/d\Theta$  where  $F$  is the frequency of the dHvA oscillation and  $\Theta$  is the angle measured from a plane perpendicular to the applied field direction. These two factors are the most important considerations when using a torque method to measure the dHvA effect. Ideally, a sample should have a large anisotropy in the dHvA frequencies and the applied field should be large. In  $\text{EuB}_6$ , the frequencies change only of order one hundred tesla through a  $45^\circ$  rotation. This fact coupled with the low field sensitivity problem inherent in the cantilever restricted us to measurements above 12 T. Additionally,  $dF/d\Theta$  for certain angles of rotation where the FS is more spherical is small, thus rendering the dHvA effect difficult to observe at low applied fields.

In the dHvA effect, the electrons contributing to the signal are exposed to the total internal field inside the sample,  $B = H_{\text{ext}} + (1 - D)4\pi M$ , where  $H_{\text{ext}}$  is the externally applied field,  $D$  the sample demagnetization factor, and  $M$  the magnetization. We performed superconducting quantum interference device (SQUID) magnetization measurements on the same sample and in the same field direction (field applied parallel to a  $\langle 100 \rangle$  aligned along the long axis of the rod) on which the pulsed field dHvA measurements were made in order to measure the magnetization of the sample. The results of these measurements only gave an approximate answer ( $\sim 10\%$ ) due to the uncertainty in the dimensions of the very small sample used. However, interesting features of the field and temperature dependence of  $M$  were observed and will be discussed below.

### III. RESULTS

#### A. Magnetization measurements

We start the discussion with the overall magnetization measurements because they have implications for the dHvA results. A complete hysteresis plot at 4.5 K, with the magnetization measured with the field applied along the  $\langle 100 \rangle$  axis when the sample had been cooled from 300 to 4.5 K in zero magnetic field, is shown in Fig. 1. The measurements started at 0.001 T. The field was increased to 5.5 T, and then decreased past 0.001 to  $-5.5$  T and back up to 0.001 T. We do not include  $H_{\text{ext}} = 0$  as a data point because of the trapped flux in the superconducting magnet at zero current in the SQUID system leaves an approximate 0.001 T field at zero current. There are several observations to be made from this data. To within the accuracy of measurement there is no hysteresis in the data, there is no zero field remnant magnetization, and as can be seen in Fig. 2, the magnetization continues to have a small positive slope at 5.5 T. Thus the coercive force in this material is exceedingly small, even zero to within the accuracy of the SQUID measurements. This means that there should be no change in the dHvA data between up and down sweeps of the pulsed field.

A final note about the shape of the magnetization versus field at constant temperature measured with the SQUID is in order. Since  $\text{EuB}_6$  has highly localized moments with spin  $S = \frac{7}{2}$ , the shape of this curve is expected to follow a Brill-

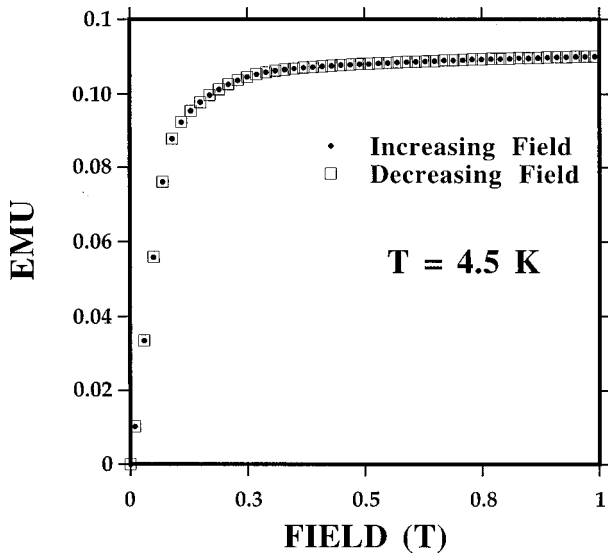


FIG. 1. Magnetization between zero and 1 T of the sample vs both increasing and decreasing applied magnetic field on the sample measured with a SQUID magnetometer.

louis function. However, we have found that this is not the case. An excellent fit is obtained from zero to 5.5 T if we add to the  $S = \frac{7}{2}$  Brillouin function what is expected from a two level spin  $\frac{1}{2}$  system having Langevin paramagnetism,  $M = N\mu \tanh(\mu B/k_B T)$  as shown in Fig. 2. This result will be discussed in conjunction with the Fermi surface models given below.

Also we have made magnetization vs field measurements to 30 T at 0.5 K in the pulsed field measurement system with greatly reduced amplifier gain from the dHvA measurement parameters. To within the accuracy of this measurement saturation is reached before 30 T and there is no hysteresis. The point of these measurements is that regardless of the spin coupling mechanism causing the ferromagnetic state in this material, at the fields and temperatures used for the

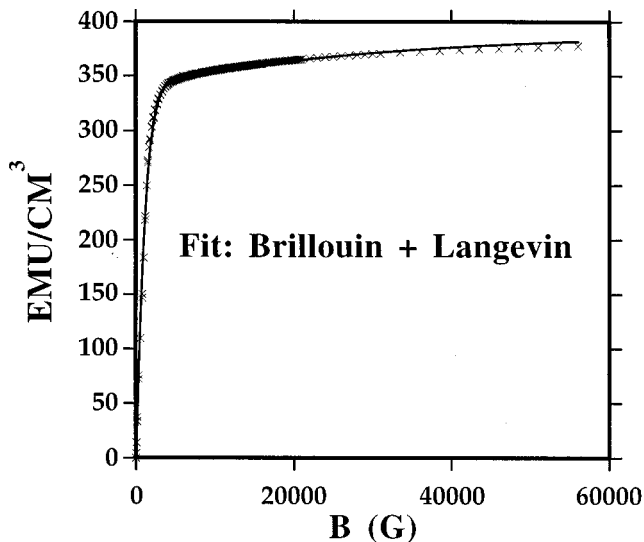


FIG. 2. Magnetization/cm<sup>3</sup> of the sample as a function of  $B$  for both increasing and decreasing applied magnetic field measured with a SQUID magnetometer. The fit to a sum of a Brillouin and Langevin function term also is shown.

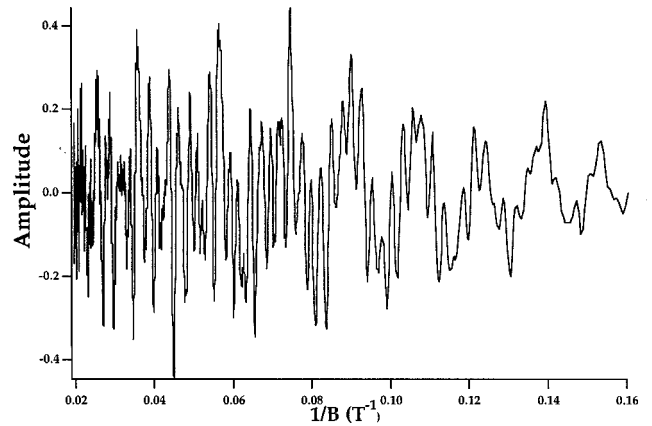


FIG. 3. Derivative of the magnetization with respect to  $B$  vs  $1/B$  at 0.4 K.

dHvA measurements the oscillating electrons are exposed to a constant internal  $B$  field, and no field-dependent corrections need to be made.

#### B. de Haas van Alphen measurements

An example of the oscillatory data from a down sweep plotted vs  $1/B$  is shown in Fig. 3. A small field region of both up and down sweep data as a function of  $B$  is shown in Fig. 4. The voltage induced in the coil by the oscillatory magnetization of the sample is given by

$$v_s = C'(dM/dB)(dB/dt),$$

and this changes sign with the changed sign of  $dB/dt$  between the up and down sweeps in a pulsed field experiment giving rise to the phase reversal in the oscillations. It is obvious that several low frequency dHvA oscillations are present in the data and it can be seen that they have the proper phase reversal for magnetization oscillations between up and down sweeps.

The data was prepared for Fourier analysis by first interpolating between data points to give a new data set that was equally spaced in  $1/B$ . Then a Hanning window was applied to these data and the Fourier analysis was calculated. To determine the frequencies and amplitudes, a discrete Fourier

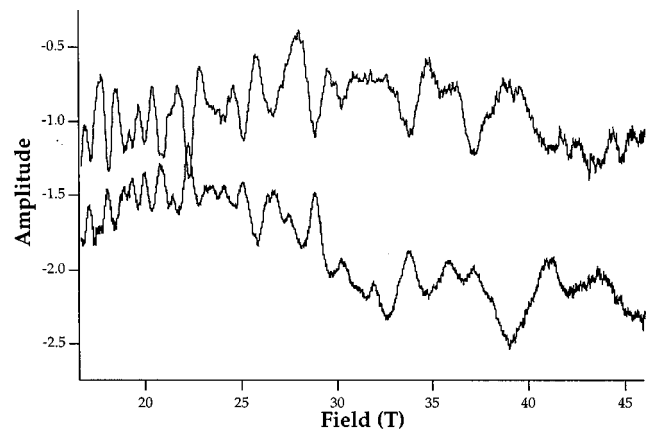


FIG. 4. Derivative of the magnetization with respect to  $B$  vs  $B$  for both increasing and decreasing field at 0.4 K. From this one can see that the proper phase reversal for dHvA occurs.

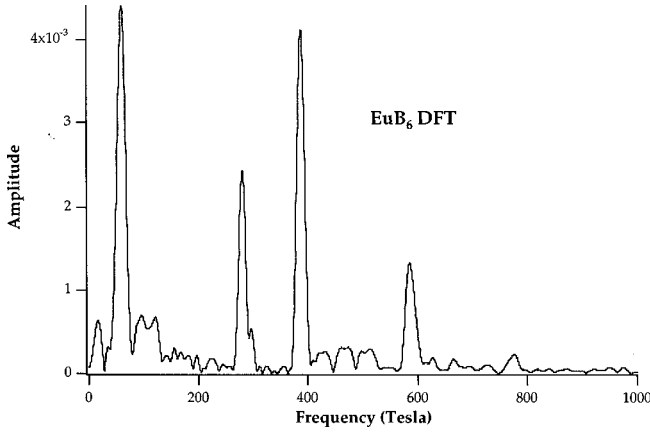
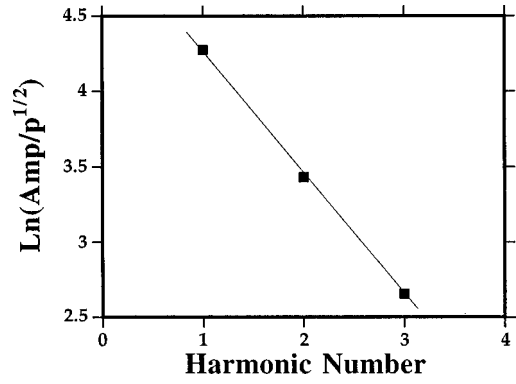


FIG. 5. Discrete Fourier transform of the data in Fig. 4.

transform (DFT) was done in which first the data from a down sweep was integrated over a wide range of frequencies (0 to 50 kT). This first integration gives a rough idea of what frequencies are present. The frequency range for the integration was then decreased to span only the observed frequencies and the resolution in frequency increased. For the final frequency determination the  $B$  field inside the sample must be used. Starting with values of  $M' = (1 - D)4\pi M$ , where  $M$  is obtained from the SQUID measurements and  $D$  is approximately 0.8 for a length to diameter ratio of 4 for this sample, a noticeable decrease in the width and increase in the amplitude of the Fourier transform peaks is obtained. This additional internal field also changes the frequencies. Thus we used  $M'$  as a single adjustable parameter to minimize the Fourier transform peak widths and maximize the amplitudes simultaneously for the measured frequencies. The final value of  $M$  obtained in this manner is within 10% of the value obtained from the SQUID measurements.

The result of this final Fourier transform using  $B$  in the analysis is shown in Fig. 5. There are four frequencies significantly above the noise level. The lowest of these frequencies (64 T) corresponds to the same orbit with a frequency of 49 T reported by Cooley<sup>6</sup> without corrections for  $M'$ . When our data is analyzed without internal field corrections we also obtain a value of 49–50 T for this orbit. We interpret these four frequencies to arise from electron and hole ellipsoids of revolution centered at the  $X$  point of the cubic BZ. Each ellipsoid has its major axis along the  $\Gamma X$  direction, and with the field along  $\langle 100 \rangle$  contributes signals from both its maximum and minimum areas.

We see no evidence of spin splitting in the data, which could be for one of two reasons. First, the Lande  $g$  factor could be of such a value ( $\pi g m / 2m_0 = q\pi$ , where  $q$  is very nearly an integer) that very little Zeeman splitting of the Landau levels occurs. Second, we could be observing single spin (spin polarized) FS sheet predicted by band theory.<sup>13</sup> From the present data we cannot definitely choose between these two possibilities for all of the frequencies, but there is evidence that the spin polarized configuration for one of the ellipsoids is correct. Our measurements extend to 50 T, and this is near the quantum limit ( $n=0$  Landau level) for the 64 T orbit. The other orbits are in Landau levels that are near the quantum limit with their being in the  $n=2$  to 12 Landau levels at the highest fields. If spin splitting were present, we should observe it for the lowest quantum numbers, even if

FIG. 6. Plot of  $\ln(A_p/p^{1/2})$  vs  $p$  for the 64 T orbit in  $\text{EuB}_6$ .

the splitting is very small. We point out that at these fields and temperatures spin splitting is easily observed in Bi,<sup>17</sup> which has a FS giving rise to similar frequencies.

The smallest of the observed orbits shows two harmonics in addition to the fundamental. When a dHvA signal from a spin polarized sheet of FS is observed the  $\ln$  of the amplitudes (divided by the square root of the harmonic number  $p$ ) of the harmonics should be proportional to the harmonic number. The exponential decay is due to the fact that for a single spin, there is no spin splitting multiplicative term  $\cos(\pi p g m / 2m_0)$ , multiplying the overall amplitude and giving nonexponential harmonic amplitudes. We show a plot of  $\ln(A_p/p^{1/2})$  vs  $p$  in Fig. 6 for the 64 T orbit, the only one for which more than one harmonic is observed. This linearity lends support to the conclusion that this sheet of FS giving rise to the lowest frequency is spin polarized.

We have measured the amplitude of each of the four frequencies measured in pulsed fields of  $H \parallel \langle 100 \rangle$  at six temperatures ranging from 0.4 to 4 K. From these temperature-dependent measurements of the signal amplitude, the effective mass  $m^*$  for each orbit can be determined. The measured values of  $m^*$  are given in Table I along with the frequencies. All of the measured values of  $m^*$  are less than one, so  $\text{EuB}_6$  cannot be put within the class of heavy fermions such as  $\text{CeB}_6$ , but if the spin polarized FS picture is correct, there are similarities in the overall configuration of the FS.<sup>18</sup> That is, the presence of localized moments near the Fermi level plays a role in the band structure.

In order to determine if our assignment of the frequencies to a FS picture is correct, we attempted angular dependent torque measurements at low fields. The field range over which signals were observed was approximately 14 to 24 T. In this range all of the frequencies observed in the pulsed field experiment with  $H \parallel \langle 100 \rangle$  were observed, but the Fou-

TABLE I. Observed dHvA frequencies, calculated areas, and effective masses in  $\text{EuB}_6$ .

Frequencies (T)	Areas (% of BZ area)	Effective masses ( $m/m_0$ )
$F_1 = 64$	0.0025	0.25
$F_2 = 282$	0.012	0.80
$F_3 = 389$	0.016	0.58
$F_4 = 588$	0.024	0.90

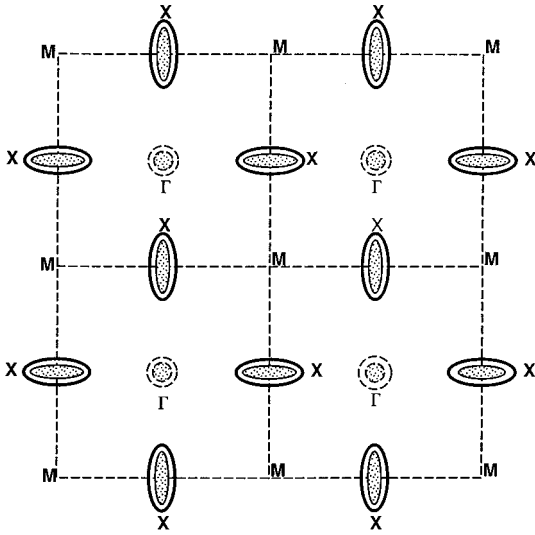


FIG. 7. Model FS of  $\text{EuB}_6$ . The larger ellipsoids are electrons, and the smaller ones holes. The circular dotted sheets above the  $\Gamma$  point are not in the same plane with the ellipsoidal shaped sheets.

rier transforms (FT) were broad due to the small number of oscillations. The lowest frequency has about four oscillations in this field range, while the highest has approximately 14. Data were obtained at eight different angles in the  $[100]$  plane. As will be discussed below, when the field is rotated from the  $\langle 100 \rangle$  six frequencies should appear, and at these intermediate fields they are not all resolved.

#### IV. DISCUSSION

The energy band calculations of Massidda *et al.*<sup>13</sup> predict two FS pockets, one electron and one hole, centered at the  $X$  point of the cubic BZ. Each of the pockets should be an ellipsoid of revolution with the longest axis extending in the  $\Gamma X$  direction. Furthermore, they predict the hole pocket to be exchange split with the up spin above the Fermi level so that the hole pockets contain down spins only. We show a model FS based on this prediction in Fig. 7. If  $\text{EuB}_6$  were a compensated metal as predicted in Ref. 13, the electron and hole pockets would be of equal volume and there would be only two dHvA frequencies. In Fig. 7 we show different size electron and hole pockets giving rise to four dHvA frequencies in agreement with our measurements for the field directed along a  $\langle 100 \rangle$ .

As the field is rotated from the  $\langle 100 \rangle$  these four frequencies should break into six branches as shown schematically in Fig. 8 for two possible assignments of frequencies to different ellipsoids. The remaining combination of frequencies leads to crossings of the electron and hole FS pockets. In either case the spectrum is complicated and we are not able to definitely choose between them due to the small number of oscillations in the low field data. The sharpest FT peak occurs from  $F_1$ , and we do observe that  $F_1$  remains approximately constant as a function of angle in addition to branching downward suggesting that the ellipsoids of revolution are the correct model. The major difference between the two models is that for model 1 the electron and hole ellipsoids more nearly have the same volume and have a larger ellipticity factor while for model 2 the volumes are substantially

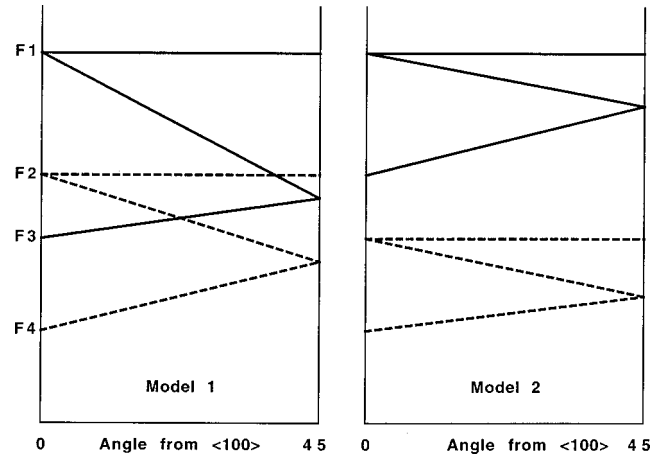


FIG. 8. Schematic representation of the angular dependence of the dHvA frequencies for field rotations in the  $[100]$  plane for the two model Fermi surfaces.

different and the ellipsoids are more nearly spherical. The band calculations give the two ellipsoids to be of equal size, with the hole ellipsoid spin polarized. Therefore, on this basis model 1 is the closest.

From the two observed frequencies the volume of the FS for both electrons and holes can be calculated using the Onsager relation  $A = (2\pi e / c\hbar) F = (9.546 \times 10^{11}) F$ , where  $A$  is the extremal cross-sectional area of the FS in  $(\text{cm})^{-2}$  and the frequency is measured in kT. For an ellipsoid of revolution, the volume  $V = (4/3)\pi abc$  of the FS is given in each case by  $V = (4/3\pi^{1/2})(A_1)^{1/2}A_2$ , where  $A_1 = \pi a^2$  is the minimum area of the ellipsoid of revolution, and  $A_2 = \pi bc$  is the maximum area. From these volumes the electron, and hole density at the Fermi energy can be calculated in each case. In Table II we show the electron density for both models. In addition to the two FS models discussed above there is the possibility that one or more of the pockets is spin polarized. This leads to additional possibilities concerning the electron density. Thus in Table II we also include values for the hole band being spin polarized, models 1A and 2A. We note that in calculating the electron densities, we use the volumes of three complete ellipsoids per BZ ( $\frac{1}{2}$  pocket per  $X$  point).

One expects the ratio of the areas measured parallel and perpendicular to the long axis of each ellipsoid to be approximately equal to the ratio of the effective masses for the two orbits. For electrons in model 1 ( $F_1$  and  $F_3$ ) the area ratio is 2.1 and the mass ratio is 1.13 whereas for model 2 ( $F_1$  and  $F_2$ ) the electron area ratio is 1.51 and the mass ratio is 1.55. For the holes in model 1 the area ratio is 6.1

TABLE II. Electron density in number per  $\text{cm}^3$  for various FS models of  $\text{EuB}_6$ .

Model	Electron density ( $n_e$ )	Hole density ( $n_h$ )	Effective density ( $n_{\text{eff}}$ )
1	$1.68 \times 10^{20}$	$2.14 \times 10^{19}$	$-6.61 \times 10^{20}$
2	$1.60 \times 10^{20}$	$1.82 \times 10^{19}$	$-3.27 \times 10^{20}$
1A	$1.68 \times 10^{20}$	$1.07 \times 10^{19}$	$-3.07 \times 10^{20}$
2A	$1.60 \times 10^{20}$	$9.12 \times 10^{18}$	$-2.26 \times 10^{20}$

with a mass ratio of 2.32 and for the holes in model 2 the area ratio is 4.4 with the mass ratio of 3.2. Thus on this basis alone, one might discount model 1.

Hall effect measurements yield values for the net carrier concentration. In order to compare with previous Hall effect measurements,<sup>4</sup> we have assumed a two band model where the net effective carrier concentration is given by  $n_{\text{eff}} = (n_h + n_e b)^2 / (n_h - n_e b^2)$ , where  $b$  is the ratio of the mobilities,  $b = \mu_e / \mu_h$ . We further assume that at low temperatures ( $< 4$  K) where our measurements were made the scattering is due to impurities and the relaxation time is constant and the same for both electrons and holes. Thus  $b$  is taken to be  $m_h^* / m_e^*$  where  $m_h^*$  and  $m_e^*$  are the appropriately averaged values of the effective mass over the ellipsoids. That is, for each ellipsoid  $1/m^* = (1/3)(1/m_{\parallel}^* + 2/m_{\perp}^*)$  where  $m_{\parallel}^*$  is measured with the field applied along the major axis of the ellipsoid, and  $m_{\perp}^*$  is measured for the field perpendicular to the major axis. The results of these calculations are given in Table II. In this calculation negative values indicate majority electrons contributing to the Hall effect. The measurements of Guy *et al.*<sup>4</sup> give a value of  $n_{\text{eff}} = -1.7 \times 10^{20}$  at 4.2 K. As can be seen for all of the models  $n_{\text{eff}}$  is negative, and model 2A gives the best agreement with the measured value. Model 2A has the largest difference between electron and hole ellipsoid volumes along with the hole ellipsoid being spin polarized. Model 1A is in the closest agreement with band calculations, but gives a factor of almost two difference for the measured  $n_{\text{eff}}$ .

The results of these models also can be compared to the measured plasma frequency of approximately  $4750 \text{ (cm)}^{-1}$  in the metallic state.<sup>7</sup> For this comparison we calculate an effective  $n/m = n_e / m_e + n_h / m_h$ , and a predicted plasma frequency  $\omega_p = (4\pi e^2 n / m)^{1/2}$ . All of the models give values between  $4450$  (model 1A) and  $4740 \text{ (cm)}^{-1}$  (model 2) with model 1 giving a value of  $4710 \text{ (cm)}^{-1}$  and model 2A giving a value of  $4540 \text{ (cm)}^{-1}$ . Thus model 2 without spin polarization gives the closest agreement in this case.

Finally we point out that a spin polarized FS would give a non-negligible contribution to the overall magnetization of the sample, although in this case this contribution would be reduced due to the fact that the number of  $S = \frac{1}{2}$  holes that are spin polarized is small compared to the number of  $S = \frac{7}{2}$  Eu atoms. Thus, a Langevin function is added to fit the overall magnetization at all fields to account for the spin polarized hole sheet. The overall function that fits the magnetization data is

$$M = N_{\text{Eu}} g_{\text{Eu}} J_{\text{Eu}} \mu_B B_J(X_{\text{Eu}}) + N_h \mu_h \tanh(X_h),$$

where

$$B(X_{\text{Eu}}) = [(2J_{\text{Eu}} + 1)/2J_{\text{Eu}}] \coth \{ [2J_{\text{Eu}} + 1]/2J_{\text{Eu}} \} x_{\text{Eu}} \\ - (1/2J_{\text{Eu}}) \coth \{ x_{\text{Eu}}/2J_{\text{Eu}} \},$$

and  $x_{\text{Eu}} = B g_{\text{Eu}} J_{\text{Eu}} \mu_B / k_B T$ ,  $X_h = B \mu_h / k_B T$ ,  $N_{\text{Eu}} = 1 =$  number of Eu atoms per unit cell,  $N_h =$  number of holes per unit cell,  $N_e =$  number of electrons per unit cell,  $T$  is the tempera-

ture, and we assume  $g = 2$  for both the Eu  $4f$  electrons and the conduction electrons. In fitting the data we have assumed a functional form as follows:

$$M = C_1 [(8/7) \coth(8C_2 B/7) - (1/7) \coth(C_2 B/7)] \\ + C_3 \tanh(C_4 B),$$

where  $B$  is the internal magnetic field,  $B = H_{\text{app}} + (1 - D)4\pi M_m$ , and the values of  $M_m$  are the measured values. In this equation, the ratio  $C_3/C_1$  is simply  $(2/7)N_h/N_{\text{Eu}}$  and we find  $N_h/N_{\text{Eu}}$  to be  $6.65 \times 10^{-4}$ , or since there is one Eu per unit cell, the hole concentration is  $6.65 \times 10^{-4}$  per unit cell. From Table II the hole density in model 2A is given to be  $9.12 \times 10^{18} \text{ (cm)}^{-3}$ , and using a lattice constant of  $4.19 \times 10^{-8} \text{ cm}$  this converts to  $N_h = 6.8 \times 10^{-4}$  per unit cell which is in excellent agreement with the magnetization measurements. All of the other models give values of  $N_h$  much larger.

## V. CONCLUSIONS

We have determined from pulsed field magnetization and low field torque dHvA measurements that the FS of EuB<sub>6</sub> consists of two pockets. We interpret these to be an electron and a hole ellipsoid both centered at the X point of the BZ as predicted by energy band calculations. The effective masses are determined and given in Table I. All of the effective masses are less than 1, so no large electron-electron interaction correction to the calculated energy bands are needed as they are in the case of heavy fermions. From the lack of observation of spin splitting in the lowest frequency data and the harmonic amplitudes of this frequency, we also conclude that the hole band is spin split with one spin state above and one below the Fermi energy. We have considered two model Fermi surfaces, both of which give ferromagnetic EuB<sub>6</sub> to be an uncompensated metal. In one model (1) the FS sizes are closest to the band calculations in that EuB<sub>6</sub> is more nearly compensated in this model. In the second model, where the ratio of the two areas are in agreement with the ratio of the two masses, the effective number of carriers are closest to the measured values with model 2 giving the best agreement with the reported plasma frequency,<sup>7</sup> while model 2A, with spin splitting of the hole band, agrees best with previous Hall effect measurements<sup>2</sup> and the magnetization measurements as a function of field. Finally, we point out that all of the models result in the material being uncompensated, whereas the band calculations are based on the premise of compensation with localized  $f$  electrons.

## ACKNOWLEDGMENTS

Much of this work was performed at the National High Magnetic Field Laboratory supported by the NSF, the State of Florida, and the U.S. Department of Energy. One of the authors (R.G.G.) acknowledges support by NSF Grant No. DMR95-01419 and also would like to thank S. von Molnar for many helpful comments. This experiment was originally suggested to R.G.G. by F. M. Mueller, and we gratefully acknowledge his input.

- <sup>1</sup>Y. Isikawa, M. M. Bajaj, M. Kasaya, T. Tanaka, and E. Bannai, *Solid State Commun.* **22**, 573 (1977).
- <sup>2</sup>Z. Fisk, D. C. Johnston, B. Cornut, S. von Molnar, S. Oseroff, and R. Calvo, *J. Appl. Phys.* **50**, 1911 (1979).
- <sup>3</sup>T. Fujita, M. Suzuki, and Y. Isikawa, *Solid State Commun.* **33**, 947 (1980).
- <sup>4</sup>C. N. Guy, S. von Molnar, J. Etairieau, and Z. Fisk, *Solid State Commun.* **33**, 1055 (1980).
- <sup>5</sup>J. M. Tarascon, J. L. Souberoux, J. Etourneau, R. Georges, J. M. D. Coey, and O. Massenet, *Solid State Commun.* **37**, 133 (1981).
- <sup>6</sup>Jason C. Cooley, Ph.D. thesis, University of Michigan, 1997; J. C. Cooley, M. C. Aronson, J. L. Sarrao, and Z. Fisk, *Phys. Rev. B* **56**, 14 541 (1997).
- <sup>7</sup>L. Degiorgi, E. Felder, H. R. Ott, J. L. Sarrao, and Z. Fisk, *Phys. Rev. Lett.* **79**, 5134 (1997).
- <sup>8</sup>Z. Fisk, *Phys. Lett.* **34A**, 261 (1971).
- <sup>9</sup>R. M. Xavier, *Phys. Lett.* **25A**, 244 (1967).
- <sup>10</sup>A. M. deGraaf and R. M. Xavier, *Phys. Lett.* **18**, 225 (1965).
- <sup>11</sup>P. Nyhus, S. Yoon, M. Kauffman, S. L. Cooper, Z. Fisk, and J. Sarrao, *Phys. Rev. B* **56**, 2717 (1997).
- <sup>12</sup>S. Süllow, I. Prasad, M. C. Aronson, J. L. Sarrao, Z. Fisk, D. Hristova, A. H. Lacerda, M. F. Hundley, A. Vigliante, and D. Gibbs, *Phys. Rev. B* **57**, 5860 (1998).
- <sup>13</sup>S. Massidda, A. Continenza, T. M. dePascale, and R. Monnier, *Z. Phys. B* **102**, 83 (1997).
- <sup>14</sup>P. T. Coleridge and I. M. Templeton, *Phys. Rev. B* **25**, 7818 (1982).
- <sup>15</sup>M. Chparala, O. H. Chung, and M. J. Naughton in *Superconductivity and Its Applications*, AIP Conf. Proc. 273, edited by H-S. Kwok, D. T. Shaw, and M. J. Naughton (AIP, New York, 1993).
- <sup>16</sup>M. J. Naughton, J. P. Ulmet, A. Narjis, S. Askenazy, M. V. Chaparala, and A. P. Hope, *Rev. Sci. Instrum.* **68**, 4061 (1997).
- <sup>17</sup>V. S. Edelman, *Adv. Phys.* **25**, 555 (1976).
- <sup>18</sup>N. Harrison *et al.* (unpublished).